GNSS-INS Fusion for Enhanced Positioning and Signal Processing in Railway Track Inspection Under Dynamic Conditions

Guang Jin[1*], Shuai Ma[2]
[1]Office of Science & Technology, Zhengzhou Railway Vocational and Technical College, Zhengzhou 451460, China
[2]School of Electrical Engineer, Zhengzhou Railway Vocational and Technical College, Zhengzhou 451460, China
E-mail: guangjin80@163.com, ms12590@sina.cn
[*]Corresponding author

Keywords: orbit detectors, global navigation satellite systems, signal acquisition, precise positioning, multi-source data

Received: April 28, 2025

The data collection and processing technology of orbit detectors and global navigation satellite systems in driving conditions is of great significance. A positioning method based on the fusion of inertial navigation system and global navigation satellite system is proposed to address the signal acquisition and fusion issues between the track inspection instrument and the global navigation satellite system during driving. This method achieves effective fusion of multi-source data through synchronous acquisition technology and time alignment algorithm, and further optimizes the data processing flow of the track inspection instrument, enhancing positioning accuracy and robustness. The experiments tested the performance of different methods in terms of positioning error, redundancy detection rate, sampling accuracy, and resource consumption by simulating three typical scenarios: open environment, urban rail transit, and mountain track. The results showed that the proposed method had an average positioning error of only 2.5 mm in an open environment, which was significantly better than the 6.2 mm error of GNSS-RTK and the 12.5 mm error of GNSS. The redundancy detection rate could reach 95.2%, which was nearly 10% higher than GNSS-RTK and 30% higher than GNSS. In urban and mountainous environments, positioning errors are kept within 6.8 and 8.5 mm, respectively. Meanwhile, the research's proposed method has improved its signal-to-noise ratio to 45.8 dB and decreased its mean square error by over 40%. This demonstrates its excellent anti-interference and denoising capabilities. The experimental results demonstrate that the proposed method significantly improves the positioning accuracy and real-time performance of the orbit detection system under complex operating conditions. The method is applicable to engineering and has significant promotional value.

Povzetek: Razvita jei metoda združevanja GNSS in INS za natančnejše pozicioniranje pri železniških tirnih pregledih, ki z večnitenim zajemom, časovno poravnavo in Kalmanovim filtrom poveča robustnost.

1 Introduction

With the rapid development of rail transportation, track inspection technology plays a crucial role in ensuring the safety of train operation and the efficiency of track maintenance [1]. Accurate and real-time track inspection can not only identify geometric changes and structural damage of the track, but also effectively predict potential safety hazards [2]. However, in complex track scenarios, track inspection technology faces many challenges. Especially in high-speed train operation or complex environments, signal occlusion, interference, and multipath effects can significantly degrade the performance of the localization system, resulting in large positioning error and data processing delays for orbit detectors. Traditional track detection methods rely on a single sensor or global navigation satellite system (GNSS) technology to detect the geometric characteristics of the track using independent positioning means [3]. Ma et al. proposed a correlation coefficient-based position calibration method designed to address position errors and offsets in multi-source orbit detection data. The method was divided into three parts, all of which were realized by a two-step procedure. Tests indicated that the method could effectively reduce the position error and improve the data alignment, and the processing time for a 1-kilometer section was 0.66s on average [4]. Sun et al. proposed a virtual track inspection technique integrating a multi-body system model for analyzing the performance of high-speed trains passing through turnouts on main lines and branch lines. The technique was validated in the spatial and wavelength domains based on inertial measurements and vehicle turnout dynamics analysis. The results indicated that zero-phase filters at 3-25 m and 1-5 m wavelengths were essential for eliminating long-wave interference and identifying turnouts [5]. Chen et al. constructed a mathematical model of the track geometry vehicle path optimization problem for periodic demand and used the modal algorithm, a meta-heuristic method, to solve it efficiently. The application of this method in a real case revealed that it was able to reduce 295.016 kilometers of ineffective mileage and significantly improve the efficiency of the maintenance cycle [6]. Zvirblis et al. examined the use of time series deep learning for conveyor

belt monitoring. They focused on analyzing how data augmentation techniques affect the accuracy of tension signal classification. By introducing various enhancement methods such as Laplacian noise, Gaussian drift noise, uniform noise, and amplitude distortion, combined with TimeVAE to generate synthetic data, experiments indicated that these techniques could effectively improve the classification performance of the model [7].

In recent years, GNSS has a wide range of applications in track detection and positioning, the core of which lies in the realization of accurate spatial positioning through satellite signals, which provides key support for the safe operation and maintenance of rail transportation [8]. A method for RF interference suppression of GNSS signals based on non-negative matrix decomposition was proposed by da Silva F B et al. The method was able to separate the interference from the GNSS signal and supported both supervised and semi-blind deployment modes. Experimental results confirmed that both schemes could effectively reduce the impact of RF interference on GNSS signals [9]. Zou et al. proposed an adaptive motion-constrained microelectromechanical system (MEMS)-assisted signal tracking technique designed to quickly restore navigation services. The technique improved the accuracy of motion state identification through fuzzy reasoning and generated virtual measurements to maintain the loose integration of GNSS/inertial navigation system (INS). Experimental results revealed that this technique recognized motion states more accurately and stayed within the tracking capability of the GNSS receiver [10]. Ichikawa et al. proposed a cost-effective GNSS interferometric reflection technique for monitoring significant wave heights and wave periods of moving vessels. The technique observed the GNSS signal amplitude by high sampling rate and estimated the lookup table using analog signal based on real wave spectrum. The method was successful in obtaining accurate estimates of wave height and wave period in practical GNSS observations of ferries [11]. Hassan et al. proposed a 3D modeling algorithm based on voluntary geographic information (VGI) for GNSS non line of sight signal detection and exclusion. This method used OpenStreetMap and Google Earth data to create a 3D building model, which is verified by observing the phase smoothing code. Experiments showed that this scheme could significantly improve horizontal positioning accuracy [12]. Finally, the study summarizes the research areas, results, and limitations of the literature review mentioned above, as shown in Table 1.

Table 1 shows that significant progress has been made in recent years in the fields of orbit detection and GNSS signal processing. However, existing methods still have limitations regarding applicable environments, system integration, and positioning accuracy assurance. Most studies lack adaptive modeling for complex track scenarios, such as those involving cities, tunnels, and mountainous areas. The practicality and deployment of these studies in track geometry detection tasks is still limited. Moreover, the positioning accuracy of GNSS is easily affected by signal occlusion and multipath effects. It performs poorly in complex orbital environments, especially. Based on this background, the study innovatively fuses GNSS and INS for positioning, and realizes efficient multi-sensor collaboration through multi-threaded acquisition technology and time alignment algorithm. At the same time, in response to the orbit detection data collected by the orbit detector, the positioning fusion process between INS and GNSS is optimized using Kalman filtering technology, which effectively improves the accuracy and efficiency of the track inspector data processing. The research aims to provide new ideas for the fusion application of track inspection instrument and GNSS, and improve the reliability and accuracy of track inspection system in complex environment.

Table 1: Literature summary table

Authors	Year	Algorithms/methods used	Key results	Limitations
Ma et al. [4]	2023	Position calibration method based on correlation coefficient	This method can significantly reduce the error between the detection data and the actual position, with an average time of only 0.66s per kilometer of road section	Only validate railway operation data
Sun et al. [5]	2023	Virtual orbit detection technology integrating multi-body system models	3-25m and 1-5m zero phase filters can effectively eliminate long wave interference and identify turnouts.	Without considering system latency or processing efficiency.
Chen et al. [6]	2024	Mathematical model of track geometry vehicle routing problem with periodic demand	Saved 295 kilometers of ineffective mileage and improved maintenance efficiency	Only applicable to pre planned path optimization scenarios
Zvirblis et al. [7]	2024	Application of time series deep learning models in signal data enhancement	Data augmentation has generally improved classification accuracy	Not suitable for direct application to GNSS
da Silva F B et al. [9]	2022	A GNSS signal RFI suppression method based on NMF.	Effectively suppress the interference of multiple RFIs on GNSS signals.	Focusing on anti-interference capability at the signal demodulation level
Zou et al. [10]	2023	MEMS assisted signal tracking method based on adaptive motion constraints	Improve the accuracy of state recognition	Only applicable to urban GNSS occlusion issues
Ichikawa et al. [11]	2024	GNSS interferometric reflection technology	Effective estimation of wave height and wave period	Only applicable to sea surface or surface platforms
Hassan et al. [12]	2022	Combining VGI to construct 3D building models for detecting and eliminating non line of sight signals	Improve horizontal positioning accuracy	Unable to adapt to complex scenarios where GNSS is unavailable

2 Methods and materials

Through multi-source data fusion technology, the research combines the high frequency and short-term accuracy of INS with the long-term reference position of GNSS to realize their complementary advantages. In addition, the Kalman filter is used to solve the results in the INS-GNSS fusion structure, achieving smooth compensation and accuracy enhancement for GNSS interruption scenarios.

2.1 Data acquisition and processing of railroad track inspector under traveling condition

The core of the rail checker in the traveling state is the data acquisition subsystem, which consists of sensor modules, data acquisition control unit, data storage, transmission module, and multi-source data fusion [13]. Synchronizing the time of multi-sensor data is crucial for coordinating them. The core of achieving this synchronization is the synchronous acquisition and data alignment algorithms. The acquisition process is shown in Figure 1 [14].

In Figure 1, the multi sensor synchronous acquisition process includes the data acquisition process of INS, GNSS, A/D signal processor, acceleration measurement module (AMS), and gauge measurement system (GMS) [15]. The data from INS and GNSS are transmitted via RS232 interface at 200Hz and 20Hz, respectively, while the AMS and instrumentation measurement module are transmitted via ICP/IP interface at 2000Hz. All data are processed by the multi-threaded acquisition system to generate INS sampling data, GNSS sampling data, and AMS, instrumentation measurement module sampling data, respectively. The integration of multi-source data from track checker needs to solve the problem of unsynchronization between devices in terms of reference, sampling frequency, time starting point, data resolution, and transmission delay. The study proposes a soft synchronization method based on UTC time to unify the timestamps, as shown in Figure 2 [16].

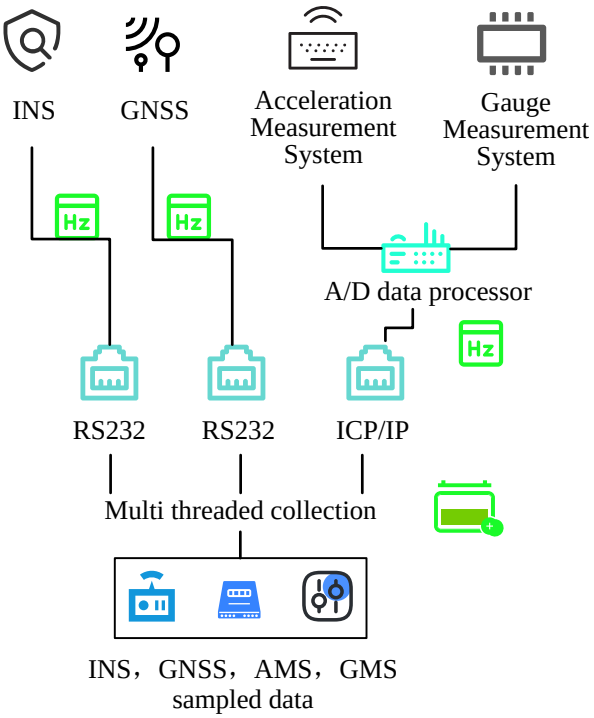

Figure 1: Multi sensor synchronous acquisition process diagram.

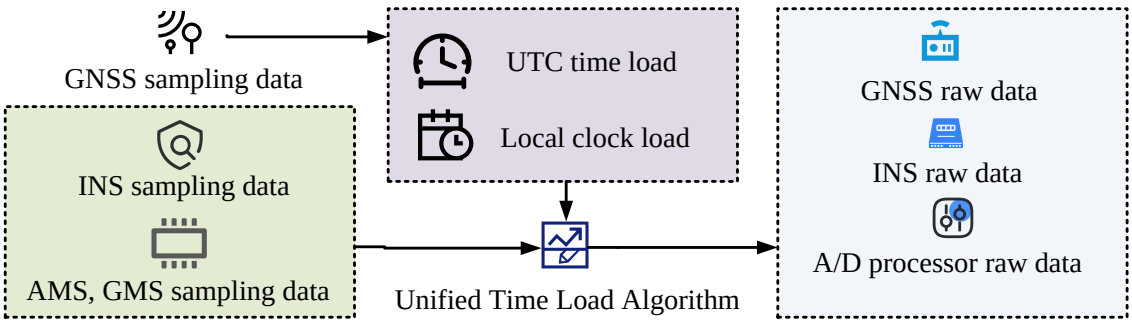

Figure 2: Time alignment process.

Figure 2 shows that during the alignment process, the system uses a UTC timestamp and a local clock signal for dual-time reference synchronization. This allows the system to accurately align original data from sensors with different sampling frequencies to a unified time benchmark. Thus, the system ensures timing consistency and fusion of the overall data. By using a second-order digital signal holder for extrapolation, time differences can be eliminated. This method can also be applied to processing AMS and GMS data. By mapping the sampling data of each module simultaneously to a unified time base, performing delay compensation, and making extrapolation predictions, the system achieved high consistency among the four channel data sources of GNSS, INS, AMS, and GMS in the time domain. The time difference calculation process is shown in Equation (1) [17].

$$\Delta T = T_{INS} - T_{UTC} = (C_{INS} - C_{UTC}) \cdot 10^{-5} + \alpha_T \cdot \frac{(C_{INS} - C_{UTC})}{(C'_{UTC} - C_{UTC})} \quad (1)$$

In Equation (1), ΔT denotes the time difference between the INS time T_{INS} and the UTC time T_{UTC}. C_{INS} denotes the count value of INS. C_{UTC} denotes the count value corresponding to the UTC time. C'_{UTC} denotes the next count value of UTC time. α_T denotes a correction factor, which is usually used to correct the error between the count values. Next, a standard linear Kalman filter is used to model the state estimation of the attitude, velocity, and position information of the INS module, thereby reducing sensor errors and drift accumulation. To reduce sensor errors, Kalman filtering technology is used to estimate the attitude and velocity states in the INS system, in order to enhance short-term navigation accuracy. A standard linear Kalman filter is selected due to the linear relationship between the state transition model and the observation model, as well as the fact that the system input is directly measurable Inertial Measurement Unit (IMU) acceleration. The state update equation is shown in Equation (2) [18].

$$\hat{\ell}_{k|k-1} = F_k \hat{\ell}_{k-1|k-1} + B_k u_k \quad (2)$$

In Equation (2), k denotes the moment. $\hat{\ell}_{k|k-1}$ denotes the predicted state vector. F_k is the state transfer matrix. $\hat{\ell}_{k-1|k-1}$ denotes the state estimate at the $k-1$ moment. $\hat{\ell}_{k-1|k-1}$ denotes the control input matrix. B_k denotes the control input matrix. u_k is the control input vector, the actual collected data is the linear acceleration provided by IMU. The definition of u_k is shown in equation (3).

$$u_k = \begin{bmatrix} a_x, k \\ a_y, k \end{bmatrix} \quad (3)$$

In equation (3), a_x represents the x-axis acceleration component measured by the IMU at time k. b represents the y-axis acceleration component measured by the IMU at time k. The prediction error covariance is shown in Equation (4).

$$P_{k|k-1} = F_k P_{k-1|k-1} + Q_k \quad (4)$$

In Equation (4), $P_{k|k-1}$ is the predicted error covariance matrix, combining process noise modeling system uncertainty. $P_{k-1|k-1}$ denotes the estimated error covariance matrix at the $k-1$ moment. Q_k is the process noise covariance matrix, $Q_k = diag(0.01, 0.01, 0.1, 0.1, 0.5, 0.5)$. Kalman gain is calculated as shown in Equation (5).

$$K_k = P_{k|k-1} H_k (H_k P_{k|k-1} + R_k)^{-1} \quad (5)$$

In Equation (5), K_k is the Kalman gain matrix. H_k denotes the measurement matrix. R_k is the measurement noise covariance matrix, $R_k = diag(1.0, 1.0, 0.5, 0.5)$. The definition of H_k is shown in equation (6).

$$H_k = \begin{bmatrix} 1 & 0 & 0 & 0 & 0 & 0 \\ 0 & 1 & 0 & 0 & 0 & 0 \\ 0 & 0 & 1 & 0 & 0 & 0 \\ 0 & 0 & 0 & 1 & 0 & 0 \end{bmatrix} \quad (6)$$

According to equation (6), GNSS measurements can provide position and velocity information. Kalman gain and observation model are used to integrate the actual measurement results of GNSS into INS prediction and update the system state. Each instrument is calibrated at the factory, and the internal computational flow of the gyroscope in a high-precision INS is shown in Figure 3 [19].

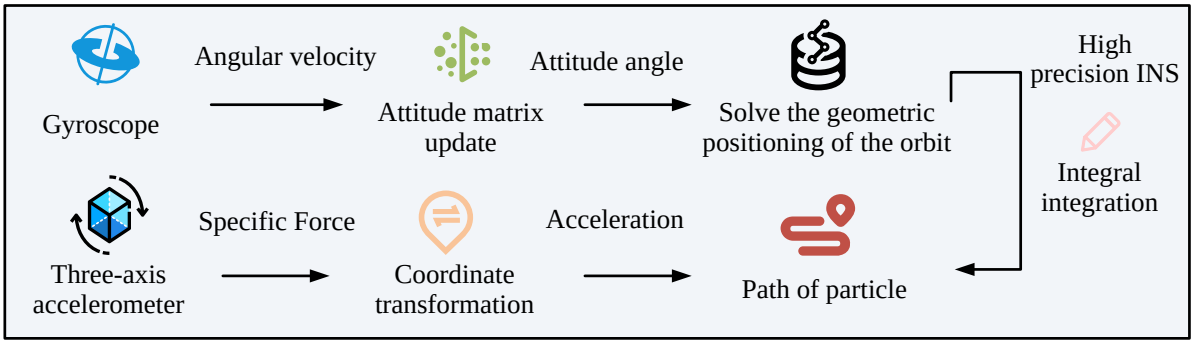

Figure 3: INS internal calculation process.

In Figure 3, the high-precision INS measures the angular velocity by means of a gyroscope to update the attitude matrix and calculate the attitude angle. Meanwhile, the three-axis accelerometer is utilized to measure the specific force, and the acceleration is obtained by coordinate transformation. The integral is used to calculate the motion trajectory, and the solution of the geometric position of the orbit is finally realized. The whole process combines the angular velocity, attitude update, and acceleration data to complete the high-precision motion state projection.

2.2 Coordinate positioning based on GNSS information fusion

To further improve the accuracy of data acquisition and processing of the rail checker under running condition, the collected GNSS information needs to be deeply fused and optimized to make up for the shortcomings and limitations of the GNSS when it is used alone. In the dynamic process of traveling, the track checker uses GNSS to provide the absolute position of the train and INS to provide short-term accurate positioning. Since GNSS signals are easily affected by the environment, they may be lost in tunnels and other areas, and the sampling frequency of GNSS is low, which cannot meet the demand for precise positioning. The study proposes a combined GNSS/INS coordinate positioning technique, which converts and corrects GNSS data to the track centerline, and combines INS data to construct a sequence of "time coordinates". To realize accurate positioning in the traveling state, GNSS is used in combination with real time kinematic (RTK) [20]. The GNSS-RTK system used by the research is based on carrier phase differential positioning to enhance accuracy. Compared to pseudorange correction, carrier phase correction provides more accurate observations and is ideal for orbit detection scenarios sensitive to positioning errors. The GNSS-RTK system used by the research is based on carrier phase differential positioning to enhance accuracy. Compared to pseudorange correction, carrier phase correction provides more accurate observations and is ideal for orbit detection scenarios sensitive to positioning errors. For areas with urban rail and tunnel access where GNSS is susceptible to multipath interference, the system introduces signal quality discrimination thresholds and satellite shielding angle screening strategies in the raw data processing layer. These strategies reduce interference from reflected signals. Taking trains as an example, the application scenario of GNSS-RTK technology is shown in Figure 4 [21].

In Figure 4, multiple satellite systems, such as GPS, BeiDou, etc., send signals to the ground, and the equipment receives the satellite signals while providing error correction values through the RTK reference station and the ground-based enhancement system. Sources of error include satellite, atmospheric, and multipath errors. Through high precision calculations and corrections from a ground-based enhancement system, positioning accuracy can be realized to a centimeter level. However, the time error that this technology can provide is only centimeter-level accuracy. Therefore, the short-term positioning advantage of INS needs to be utilized to supplement the missing part of GNSS signals, while GNSS is used to suppress the long-term drift of INS. The INS-GNSS coupling structure is shown in Figure 5 [22].

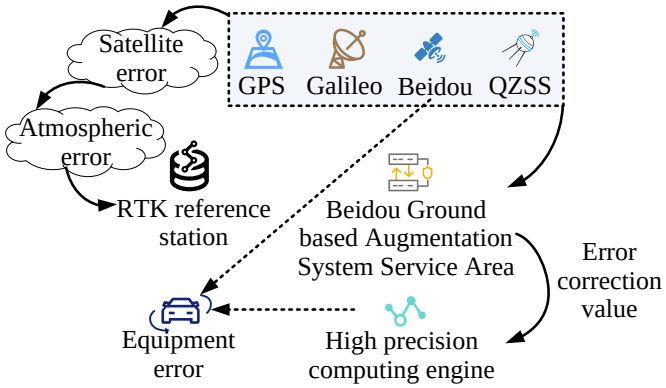

Figure 4: Principles of GNSS-RTK technology.

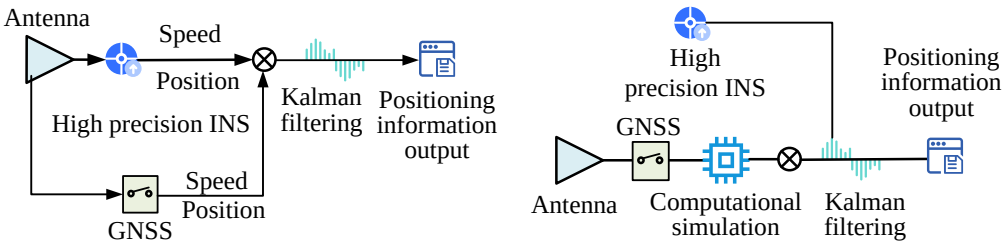

(a) INS/GNSS composite structure (b) INS/GNSS tight combination structure

Figure 5: INS-GNSS coupling structure.

Figures 5(a) and 5(b) show two fusion structures of the INS-GNSS system: the loose-coupled structure and the tight-coupled structure, respectively. In the loosely-coupled structure, the INS system and the GNSS system output velocity and position information independently, respectively. The results of both are fused by a Kalman filter to generate the position information output. In the tight combination structure, the pseudorange and carrier phase data from GNSS are directly combined with the solved results from INS. Then the Kalman filtering is used to realize a more accurate positioning information output. The study uses a loosely coupled structure to fuse the INS and multi-constellation GNSS boards in the rail checker to meet the design requirements of the miniature airborne combined positioning system. The study employs a loosely coupled structure that fuses GNSS position and INS data via Kalman filtering. This approach significantly reduces system complexity while ensuring accuracy. This fusion structure is directly compatible with commercial GNSS modules and standard IMUs. It eliminates the need to process raw observation data and can automatically switch to INS calculation mode when GNSS is interrupted. This feature perfectly meets the engineering requirements of miniaturized airborne equipment. INS utilizes inertial sensors to calculate the position, velocity and attitude of the carrier, and the acceleration of the object in the inertial navigation coordinate system is shown in Equation (7).

$$\begin{cases} V_x^n = f^n - a_x^n \\ V_y^n = f^n - a_y^n \\ V_z^n = f^n - a_z^n - g \end{cases} \tag{7}$$

In Equation (7), V_x^n, V_y^n, and V_z^n denote the velocity components of the object along the x, y, and z axes in the inertial navigation coordinate system, respectively. f^n denotes the external force component on the object in the inertial navigation coordinate system. a_x^n, a_y^n, and a_z^n denote the acceleration components in the inertial navigation coordinate system. g is the gravitational acceleration. After calculating V_x^n, V_y^n, and V_z^n, the velocity of the object to the ground is obtained by integrating once, as shown in Equation (8) [23].

$$\begin{cases} V_x^g(t) = V_x^g(0) + \int_0^t V_x^g(t)dt \\ V_y^g(t) = V_y^g(0) + \int_0^t V_y^g(t)dt \\ V_z^g(t) = V_z^g(0) + \int_0^t V_z^g(t)dt \end{cases} \tag{8}$$

In Equation (8), t denotes the time difference between two consecutive localization points. $V_x^g(t)$, $V_y^g(t)$, and $V_z^g(t)$ denote the variation of the object's velocity with t in the x, y, and z-axis directions in the inertial navigation coordinate system, respectively. $V_x^g(0)$, $V_y^g(0)$, and $V_z^g(0)$ denote the last localization point of the object in the x, y, and z axis directions that recorded the carrier's velocity to the ground before the GNSS signal is interrupted, respectively. Subsequently, the velocity of each localization point in the INS is calculated as shown in Equation (9).

$$V_i = V_{i-1} + a_{i-1} \cdot t \tag{9}$$

In Equation (9), V_i denotes the velocity of the current localization i. V_{i-1} denotes the velocity of the last localization of i. a_{i-1} denotes the acceleration of the last localization of i. The flow of INS accurate latitude and longitude update is shown in Figure 6.

In Figure 6, first, INS outputs the specific force data and removes the harmful acceleration through the conversion matrix, followed by latitude and longitude unit conversion and defining the relevant parameters. Next, the navigation belt number and the central meridian longitude are calculated, and the results are substituted into the latitude and longitude coordinate conversion formula. According to the coordinates and velocities of the initial points, the acceleration of each detection points under the navigation coordinate system and the position information based on the acceleration and velocity are calculated. The precise coordinates of the detected points are finally output.

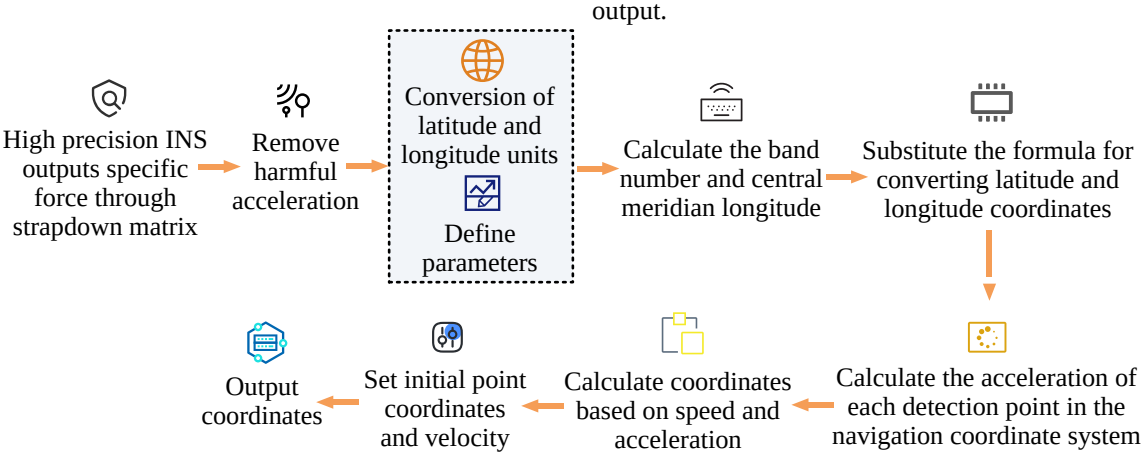

Figure 6: The process of updating INS precise latitude and longitude.

Table 2: Data processing performance results.

Collection method	Scene	SNR (dB)	MSE (mm)	Data denoising effectiveness (%)	MSE standard deviation
GNSS	Open environment	35.2	0.8	75.6	0.15
	Urban rail transit	25.3	1.5	65.2	0.25
	Mountain track	18.7	2.3	50.8	0.28
GNSS-RTK	Open environment	40.1	0.5	80.1	0.12
	Urban rail transit	30.5	1.2	70.5	0.18
	Mountain track	20.2	2.1	60.2	0.25
Ours	Open environment	45.8	0.3	90.3	0.08
	Urban rail transit	38.9	0.8	85.2	0.13
	Mountain track	32.4	1.5	78.5	0.21

3 Results

The study analyzes the performance of the proposed INS-GNSS fusion method in data processing and GNSS signal positioning for the rail checker under traffic conditions. Simulation experiments are carried out in three typical scenarios: an open environment, urban rail transit, and a mountain track. The performance of the three methods in terms of data processing and positioning effect is compared.

3.1 Data processing performance test of railroad track checker under traveling condition

The data processing performance of the track gauge under driving conditions is tested by simulating three different scenarios: open environment, urban orbit, and mountainous orbit. GNSS, GNSS-RTK, and the fusion algorithm proposed by the research method are used to collect and process data in three different scenarios. The data collected includes 3 lines and 9 track sections, with a total trajectory length of approximately 18.6 kilometers and approximately 61000 sets of data frames. The sampling frequency of the GNSS module is 10 Hz, and the sampling frequency of the IMU inertial measurement unit is 100 Hz. The signal-to-noise ratio (SNR), mean squared error (MSE), and acquisition accuracy are used as evaluation indicators. To further evaluate the stability of each positioning method in different orbit scenarios, the standard deviation of MSE is used as the evaluation indicator. All results are the average of 5 independent experiments. The standard deviation represents the amplitude of the MSE fluctuation in different experimental rounds and reflects the stability of the positioning error. The study employs an SNR threshold filtering strategy when calculating denoising indicators. Since the GNSS module's error significantly increases when the SNR is below a certain value, the signal discrimination threshold is set to 23 dB according to the receiver manufacturer's recommendation. If the SNR at a sampling point is below 23 dB, the measurement is considered invalid and excluded from the denoising rate calculation. If the ratio is higher than 23 dB, the signal is valid and can be used for fusion and error calculation. The data processing performance results are shown in Table 2.

Table 2 shows that in open environments, the proposed method has the highest SNR of 45.8 dB, demonstrating its advantage in improving signal quality. The SNR of GNSS-RTK is 40.1 dB, which is lower than the method proposed by the research but higher than that of GNSS alone. The method proposed by the research has the lowest MSE, at 0.3 mm, indicating that it can provide higher positioning and data processing accuracy in open environments. With a standard deviation of only 0.08 mm, the MSE is significantly smaller than GNSS and GNSS-RTK. This indicates that the MSE's positioning performance is more stable under high SNR conditions. The MSE of GNSS-RTK is 0.5mm, and the MSE of GNSS is 0.8mm, both of which are inferior to the methods proposed by the research. Additionally, the proposed method by the research has the best denoising effect, reaching 90.3%. This indicates that the algorithm can eliminate noise to the greatest extent possible. In urban rail transit, the SNR of the proposed method is 32.4 dB, significantly higher than GNSS-RTK and GNSS. This indicates that the algorithm has stronger adaptability to complex environments. The GNSS method has significant error fluctuations due to signal occlusion and multipath interference, with a standard deviation of 0.20 mm. However, the MSE of the proposed method is 0.8mm, and the error fluctuations are effectively controlled within 0.13 mm. In mountainous areas, GNSS's MSE is highest at 2.3 mm. The standard deviation is also high at 0.28 mm, indicating severe environmental interference and extremely unstable positioning accuracy in complex terrain. The MSE of the method proposed by the research is 1.5mm, and the standard deviation is controlled within 0.21 mm through the INS compensation mechanism, which has stronger robustness and stability. Additionally, the SNR of the proposed method increased by an average of 2.3 to 3.5 decibels (dB), which reduced the fusion fluctuations caused by GNSS noise mismatch. This indicates that soft synchronization and parallel acquisition positively affect system stability and real-time performance. Soft synchronization achieves non-blocking data alignment between the GNSS and the IMU through timestamp alignment and a cache queue. This avoids the waiting delay caused by traditional hardware-triggered synchronization. Multi-threaded acquisition enables the GNSS, IMU, and data preprocessing channels to run simultaneously, which significantly reduces acquisition latency. In urban rail transit and mountain track, the denoising effect of fusion of the proposed method is studied to be 85.2% and 78.5% respectively, which is significantly better than the other two methods. The train running time is set to 500s, and the change of detection

resolution in different scenarios is reflected by the data sampling accuracy, as shown in Figure 7.

Figure 7(a), Figure 7(b), and Figure 7(c) show the variation of sampling accuracy of the three localization methods with the running time of the train in different scenarios, respectively. Figure 7(a) shows that GNSS sampling accuracy is about 0.25 mm and remains stable throughout the running time. However, it is lower than GNSS-RTK sampling accuracy, which is about 0.12 mm and significantly better with less fluctuation. It shows that RTK can effectively improve the sampling accuracy in open environment. The sampling accuracy of the proposed method in the study is the highest, about 0.06mm, and has the least variation, showing great stability. In Figure 7(b), the sampling accuracy of GNSS decreases to about 0.22mm and fluctuates slightly with running time. The sampling accuracy of GNSS-RTK is about 0.15mm, which is more stable but decreases compared to open environment. The sampling accuracy of the proposed method is about 0.09mm, which is still the best performance and the variation is very small. Similarly, in Figure 7(c), the sampling accuracy of the proposed method is about 0.11mm, and the fluctuation is minimized, which is significantly better than the other two methods. This indicates that the proposed fusion method effectively compensates the GNSS signal occlusion problem by INS in the mountain track and shows strong robustness. The distribution of positioning error is shown in Figure 8.

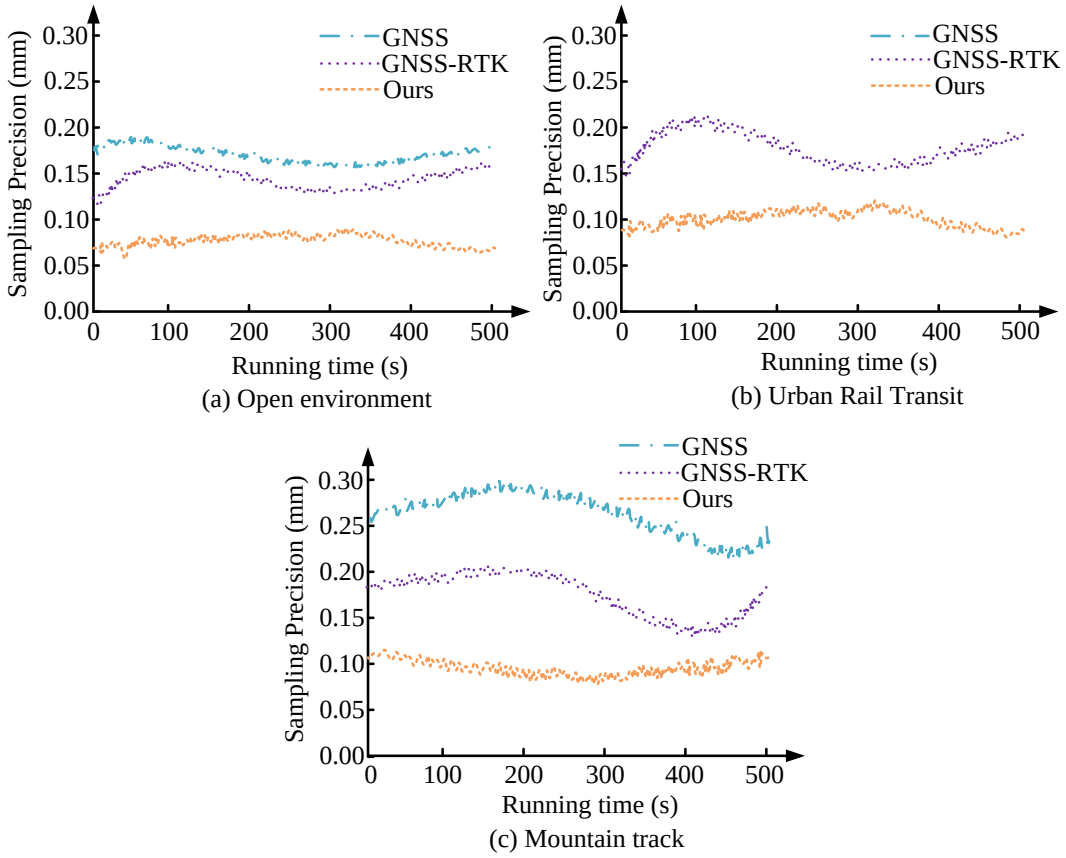

Figure 7: Detection resolution in different scenarios.

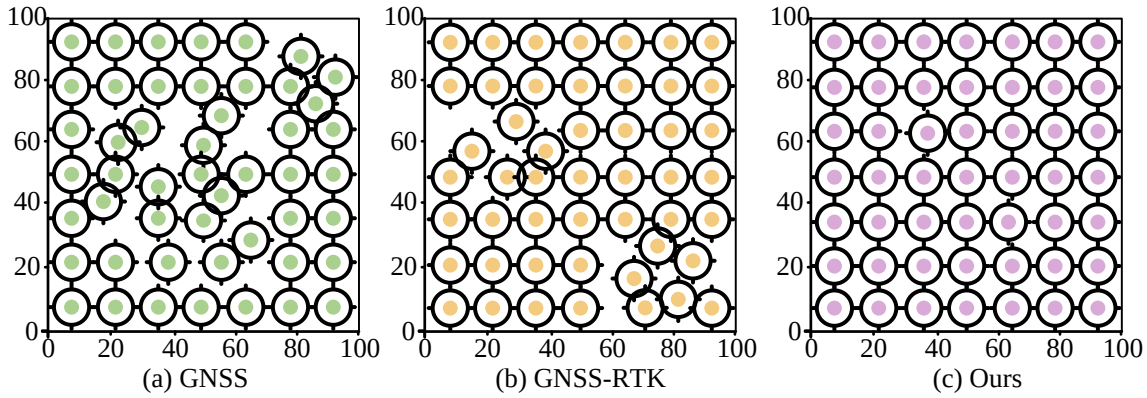

Figure 8: Distribution of positioning errors.

Table 3: Cross validation results under different speed conditions.

Method	Test Condition	Sampling Precision ± σ (mm)	Positioning Error ± σ (mm)
GNSS	30 km/h	0.29 ± 0.07	13.3 ± 1.6
	50 km/h	0.30 ± 0.08	13.0 ± 1.8
	70 km/h	0.28 ± 0.08	13.1 ± 1.9
GNSS-RTK	30 km/h	0.22 ± 0.05	6.7 ± 1.2
	50 km/h	0.23 ± 0.06	6.8 ± 1.1
	70 km/h	0.24 ± 0.07	6.9 ± 1.3
Ours	30 km/h	0.12 ± 0.04	2.9 ± 0.6
	50 km/h	0.13 ± 0.04	2.8 ± 0.6
	70 km/h	0.12 ± 0.03	2.9 ± 0.7

Table 4: Redundancy detection rate and positioning error results.

Method	Scene	Redundancy detection rate (%)	Positioning error ± σ (mm)
GNSS	Open environment	65.2	12.5 ± 1.8
	Urban rail transit	45.8	30.1 ± 2.7
	Mountain track	35.2	45.6 ± 3.1
GNSS-RTK	Open environment	85.6	6.2 ± 1.1
	Urban rail transit	78.5	12.8 ± 1.9
	Mountain track	70.3	20.5 ± 2.2
Ours	Open environment	95.2	2.5 ± 0.6
	Urban rail transit	92.1	6.8 ± 1.0
	Mountain track	90.3	8.5 ± 1.3

In Figure 8, (a), (b), and (c) respectively show the distribution of positioning performance of GNSS, GNSS-RTK, and the proposed method. Figure 8(a) shows an uneven distribution of GNSS positioning points with significant overlap and offset. The error fluctuates greatly due to multipath effects. In Figure 8 (b), GNSS-RTK significantly reduces the error range through differential correction. In Figure 8 (c), the distribution of positioning points is extremely uniform, with no significant error offset or overlap. The proposed method achieves high-precision positioning with uniform distribution and no offset through multi-source data fusion and INS compensation. This method demonstrates superior robustness in complex environments. To verify the generalization ability and speed stability of the model, cross validation is conducted under three speed conditions of 30/50/70 km/h. The results are shown in Table 3.

According to Table 3, the GNSS method maintains a sampling accuracy of 0.28-0.30 mm and a positioning error of 13.0-13.3 mm within the speed range of 30-70 km/h. The impact of speed changes on performance is relatively small, and the standard deviation of sampling accuracy and positioning error fluctuates between 0.07-0.08 mm and 1.6-1.9 mm. It indicated that the method has speed robustness but limited overall accuracy. The GNSS-RTK method has significantly improved compared to basic GNSS. The sampling accuracy increased to the range of 0.22-0.24 mm, positioning error reduced to 6.7-6.9 mm, and standard deviation controlled at 0.05-0.07 mm and 1.1-1.3 mm. It demonstrates the effectiveness of differential correction. The proposed method performs the best at all testing speeds, with a sampling accuracy of 0.12-0.13 mm, a positioning error of only 2.8-2.9 mm, and the smallest standard deviation. At a speed of 70 km/h, it can maintain a sampling accuracy of 0.12 mm and a positioning error of 2.9 mm with no significant increase in standard deviation. This fully demonstrates the stability and accuracy advantages of this method at different speeds.

3.2 Analysis of the actual effect of INS-GNSS fusion-based positioning

To evaluate the practical effect of the proposed INS-GNSS fusion method for localization in different scenarios, the study conducts simulation experiments in three typical scenarios: open environment, urban rail transit, and mountain track. The positioning error, redundancy detection rate, trajectory reconstruction accuracy, and resource consumption are tested. Similarly, the average of each set of data is based on 5 independent experiments. The standard deviation is used to measure the range of fluctuation in positioning error, which reflects the method's stability under different operating conditions. The results of redundancy detection rate and positioning error in different scenarios are shown in Table 4.

In Table 4, in open environments, the redundancy detection rate of GNSS is 65.2%, the positioning error is 12.5mm, and the standard deviation is 1.8mm. The GNSS-RTK's redundancy detection rate increases to 85.6%, and its positioning error significantly decreases to 6.2 mm with a standard deviation of 1.1 mm. The proposed method has the highest redundancy detection rate of 95.2%, with the smallest positioning error and standard deviation of 2.5mm and 0.6mm, respectively. When combined with INS, the utilization rate and positioning accuracy of redundant information improve further. In urban rail

environments, GNSS positioning errors fluctuate significantly due to multipath effects and severe GNSS occlusion. Among them, the redundancy detection rate of GNSS decreases to 45.8%, the positioning error increases significantly to 30.1mm, and the standard deviation reaches 2.7mm. The redundancy detection rate of GNSS-RTK is 78.5%, the positioning error is 12.8mm, and the standard deviation is controlled at 1.9mm. This indicates that differential technology has limited effectiveness in complex environments, but it is still significantly better than GNSS alone. The redundancy detection rate of the method proposed by the research is 92.1%, the positioning error is 6.8mm, and the error fluctuation is compressed to 1.0mm. This indicates that the method compensates for the instability of GNSS signals through inertial navigation and maintains high accuracy and robustness in complex environments. Finally, in a mountainous orbit, GNSS has the lowest redundancy detection rate, at only 35.2%. The positioning error also increases significantly, to 45.6 mm, with a maximum standard deviation of 3.1 mm. The complex terrain and severe signal obstruction in mountainous orbit environment greatly reduce the GNSS positioning effect. The redundancy detection rate of GNSS-RTK is 70.3%, with a positioning error of 20.5mm and a standard deviation of 2.2mm. Although differential technology has improved, the mountainous environment has a significant impact on signal quality. The research's proposed method significantly improves positioning accuracy and redundancy utilization through inertial navigation compensation. The measurement results show that this method has a 90.3% redundancy detection rate, an 8.5 mm positioning error, and a 1.3 mm standard deviation. These results verify the INS's effective compensation ability and the filtering strategy's robustness. The Kalman filter used in the study not only performs weighted smoothing on GNSS pseudoranges, but also estimates and corrects attitude and velocity errors of inertial measurement units. When GNSS positioning calculations are interrupted, the filter recursively calculates based on previous GNSS states and current inertial measurement values to achieve continuous positioning output. The resource consumption results during the positioning operation are shown in Figure 9.

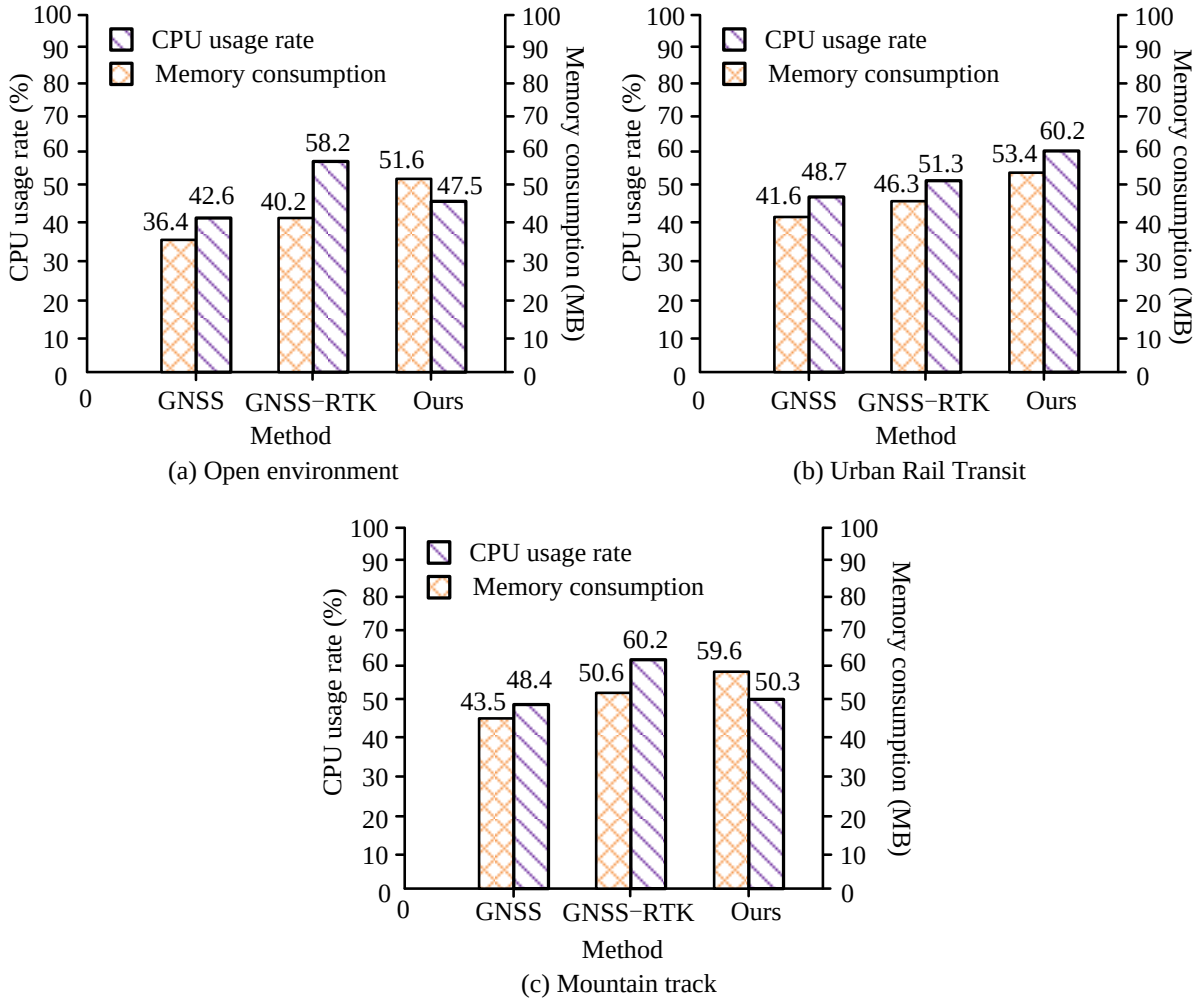

(a) Open environment

(b) Urban Rail Transit

(c) Mountain track

Figure 9: Resource consumption results.

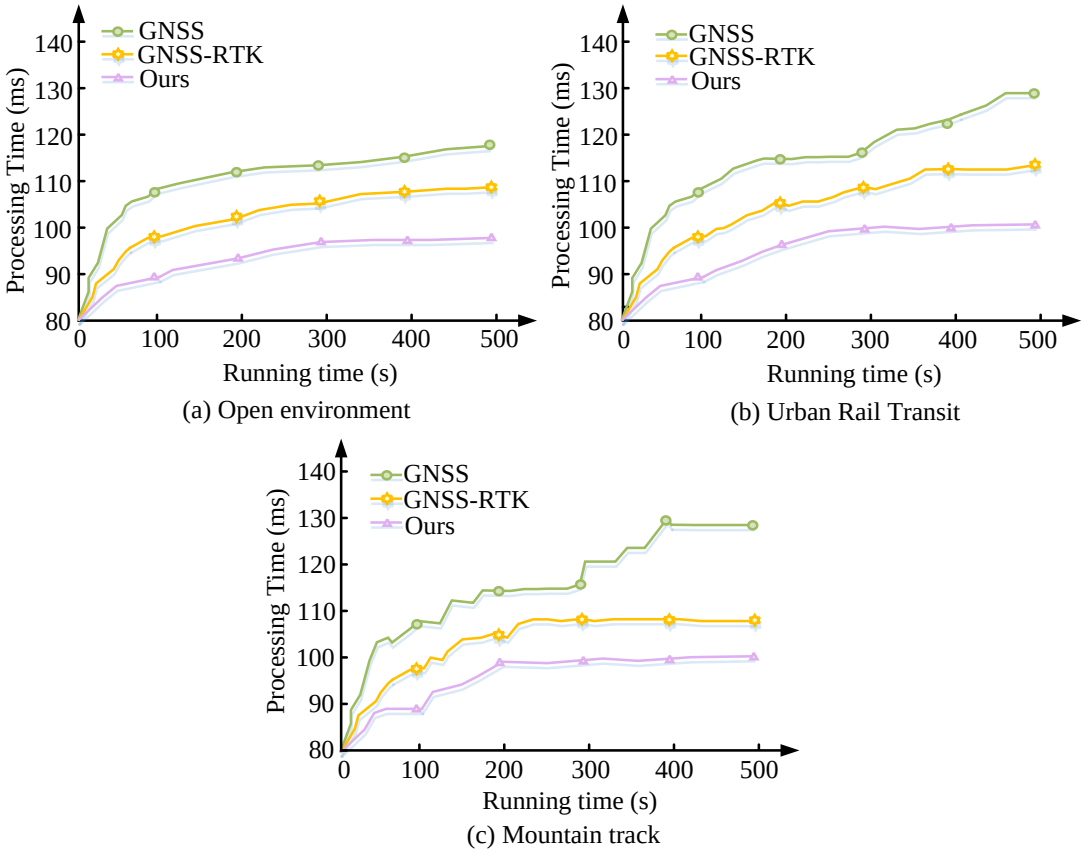

Figure 10: According to the variation of processing time with running time.

In Figure 9, (a), (b), and (c) show the comparison of CPU utilization and memory consumption of the three methods in different scenarios, respectively. Figure 9(a) shows that the GNSS method has the lowest resource utilization. It has a CPU usage rate of 36.4% and a memory usage of 40.2 MB, which indicates its low algorithm complexity. Due to differential correction, the GNSS-RTK method requires additional calculations, resulting in a CPU usage rate of 42.6% and a memory usage of 47.5 MB. The proposed method has the highest resource overhead due to multi-source data fusion and synchronization mechanism, with a CPU of 58.2% and a memory of 51.6MB. In Figure 9(b), the GNSS method has a CPU utilization of 41.6% and a memory consumption of 46.3MB, which is slightly increased by the urban rail transit signal complexity. The GNSS-RTK method has a CPU utilization of 48.7% and a memory consumption of 53.4MB, which is an increase in computational resource requirements. The CPU utilization of the proposed method in the study is 60.2%, while the memory consumption is up to 60.2MB, and the demand for multi-source data fusion is elevated in complex environments. In Figure 9(c), the GNSS method has a CPU utilization of 43.5% and memory consumption of 48.4MB, and there is an increase in the demand for memory due to the complexity of mountain signals. The CPU utilization of the GNSS-RTK method is 50.6%, which is about 7% higher than that of GNSS, and the memory consumption is 59.6MB. Differential processing has improved the complex terrain. The method proposed by the research requires inertial navigation compensation and complex terrain data fusion. This method has a CPU utilization rate of 59.6% and the highest memory consumption, at 60.3 MB. Finally, the real-time data processing is evaluated and the results are shown in Figure 10.

Figure 10(a), Figure 10(b), and Figure 10(c) show the trend of data processing time with running time for the three localization methods in different environments, respectively. Among them, the data processing time of GNSS gradually increases under the open environment in Figure 10(a). Compared with GNSS, the time of GNSS-RTK is shorter, which indicates that the differential correction effectively reduces the processing time of data errors. The starting processing time of the proposed method in the study is the lowest and slowest growing, stabilizing below 100ms. It shows that the processing efficiency of the proposed method fusion is the highest in open environment. In Figure 10(b), the processing time of GNSS increases significantly and gradually grows to 130ms. The processing time of GNSS-RTK grows to 120ms and then stabilizes. The starting processing time of the proposed method is still the lowest and finally stabilized at 105ms. It shows that the proposed method fusion can effectively improve the processing efficiency and reduce the effect of GNSS signal interference in complex environments. In Figure 10(c), the processing time of GNSS grows most significantly, from 100ms to more than 140ms. In mountainous environments, the GNSS method requires more time to process lost or unstable signals due to signal occlusion and complex

terrain. The processing time for GNSS-RTK grows to 125 ms. Although the RTK differential correction can mitigate some signal interference, it still suffers from signal multipath effects in mountainous environments. The processing time of the proposed method grows the slowest and eventually stabilizes within 110ms. It shows that the proposed method effectively controls the processing time by compensating the GNSS signal missing problem through inertial navigation in mountainous environments. To verify the robustness of the INS-GNSS fusion method in the presence of noisy, multipath interference, and occlusion data in actual rail operating environments, on-site data is collected from three real rail lines in a city's rail transit system. The results are shown in Table 5.

According to Table 5, severe satellite signal obstruction in urban subway environments significantly reduces the performance of traditional GNSS positioning. The GNSS method's average positioning error reaches 41.5 mm, with a maximum error of 54.9 mm and a signal interruption rate of up to 89.4%. Although GNSS-RTK has slightly improved through differential correction, its average error still reaches 24.6 mm, the maximum error is close to 50 mm, and the interruption rate is as high as 72.5%. In contrast, the method proposed by the research not only controls the average error at 6.4mm, but also has a maximum error of only 12.1mm. It significantly reduces the interruption rate to 17.5%, achieving fast positioning recovery in 8.9 s. This demonstrates its excellent continuous tracking capability and anti-interference performance. In the elevated line section, the average positioning error of GNSS is 18.7mm, with a maximum error of 40mm. Although GNSS-RTK technology optimizes the average error to 9.6mm, there is still an 8.7% interruption probability. The method proposed by the research further controls the error within 4.2 mm, with a maximum error of only 8.9 mm. At the same time, the interruption rate is reduced to an extremely low 1.2%, and the positioning recovery time is shortened to 0.6 seconds. In mountainous railway sections, the average positioning error is as high as 32.5 mm due to severe satellite obstruction. The maximum error is 64.8 mm, and the interruption rate remains high at 35.6%. GNSS-RTK technology has improved the average error to 17.8mm, but the signal interruption rate remains high at 18.9%. The proposed method effectively controls the average error within 8.5 mm, reduces the interruption rate to 5.4%, and enables a quick recovery in 1.1 seconds via inertial navigation compensation. This demonstrates the method's reliability and robustness in complex environments.

4 Discussion

The INS-GNSS fusion-based orbit detection and positioning method proposed in the study showed significant advantages in addressing issues such as GNSS signal occlusion and multipath effects in complex orbit environments. Experimental data showed that, on average, the positioning error of the proposed method was controlled within 10 mm in three typical environments. In an open environment, the error was only 2.5 mm, which was better than GNSS-RTK and traditional GNSS. Additionally, the traditional GNSS scheme achieved an MSE of 2.3 mm and a denoising effect of only 50.8% at an SNR of 18.7 dB. However, even in complex terrain, the research's proposed method improved the SNR to 32.4 dB, reduced the MSE to 1.5 mm, and increased the denoising rate to 78.5%. This significantly suppressed signal multipath interference. Further analysis of sampling accuracy revealed that GNSS sampling errors fluctuate around 0.25 mm in mountainous scenes. The sampling accuracy of the method proposed by the research remained stable at 0.11 mm and did not significantly deteriorate over time, which verified the role of the multi-threaded acquisition and soft synchronization mechanisms in maintaining system stability. Compared to the research by Ma et al. [4], which was based on multi-source data location calibration, the proposed method expanded its applicable environment and improved its sampling stability. It utilized redundant information more effectively and controls errors better in urban and mountainous scenarios, improving system stability. The standard deviation of the positioning error was ±1.3 mm. This was significantly better than GNSS and GMSS-RTK. It indicated that the algorithm was less volatile during dynamic orbit operations. In the speed robustness test, the GNSS-RTK error increased to 6.9 mm at 70 km/h. Meanwhile, the error remained at 2.8-2.9 mm with a standard deviation of 0.6-0.7 mm for the proposed method, further confirming its adaptability to high-speed operating environments. From a practical application standpoint, the method proposed by the research decreased the GNSS signal interruption rate in urban subways from 89.4% to 17.5% and reduced the maximum positioning error from 54.9 mm to 12.1 mm. In mountainous areas, recovery time was reduced to 1.1 s. Compared to the MEMS-based GNSS continuous tracking method proposed by Zou et al. [10], the method proposed by the research optimized the continuity of GNSS signals in discontinuous scenarios and enhanced the ability to respond quickly to occluded environments. The results indicated that this method effectively used INS to provide robust compensation for short-term signal interruptions and took full advantage of the global accuracy of GNSS.

Table 5: Comparison of actual application effects.

Scenario Type	Method	Average positioning error (mm)	Maximum error (mm)	Interruption rate (%)	Recovery latency (s)
Urban subway section	GNSS	41.5	54.9	89.4	4.9
	GNSS-RTK	24.6	48.9	72.5	3.6
	Ours	6.4	12.1	17.5	8.9
Elevated Line Section	GNSS	18.7	39.4	18.2	2.5
	GNSS-RTK	9.6	21.3	8.7	1.7
	Ours	4.2	8.9	1.2	0.6
Mountain route section	GNSS	32.5	64.8	35.6	5.1
	GNSS-RTK	17.8	38.2	18.9	2.4
	Ours	8.5	16.4	5.4	1.1

5 Conclusion

In response to the issues of large positioning errors and unstable signal quality encountered by rail checkers and GNSS systems in complex track environments, the research proposed an INS-GNSS fusion positioning method. It achieved efficient fusion of multi-source data and noise suppression by combining multi-sensor synchronous acquisition technology, time alignment algorithms, and Kalman filtering algorithms. Additionally, the effects of the track checker and GNSS signal positioning were analyzed under running conditions. The results of the experiment showed that the proposed method outperformed the other two comparative methods in all scenarios. The application verification of this method in typical orbital scenarios showed that it was significantly superior to traditional GNSS and GNSS-RTK schemes in terms of sampling accuracy, positioning error control, signal stability, and system response capability. It had good adaptability and promotion value. This method was particularly suitable for environments where tracks were operated under conditions of frequent signal obstruction, complex terrain, and significant dynamic interference. It could effectively support the efficient detection, operation, and maintenance of track facilities. In terms of resource consumption, the proposed method had slightly higher memory and CPU utilization than the traditional method. However, its processing efficiency and stability were significantly better. It could be suitable for scenarios with high real-time requirements in complex environments. Given the higher memory and computation requirements of the proposed method, future research should focus on optimizing the algorithm's efficiency and reducing resource consumption to adapt to a wider range of applications.

List of abbreviations

GNSS: Global Navigation Satellite System
INS: Inertial Navigation System
UTC: Coordinated Universal Time
RS232: Recommended Standard 232
ICP: Inductively Coupled Plasma
IP: Intellectual Property
RTK: Real Time Kinematic
GNSS-RTK: Global Navigation Satellite System-Real Time Kinematic
INS-GNSS: Inertial Navigation System-Global Navigation Satellite System
SNR: Signalto Noise Ratio
MSE: Mean Squared Error

Funding

The research is supported by 2024 Science and Technology Research Projects in Henan Province; Research and Application of Railway Track Irregularity Online Fault Detection System Based on Vibration Mechanism Characteristics (242102240130), Key Research Project of Universities in Henan Province in 2025, Research and Application of Key Technologies for High-Speed Rail Track Online Fault Detection System Based on Transfer Learning (25A580011).

References

[1] Wenbo Zhao, Weile Qiang, Fei Yang, Guoqing Jing, and Yunlong Guo. Data-driven ballast layer degradation identification and maintenance decision based on track geometry irregularities. International Journal of Rail Transportation, 12(4):581-603, 2024. https://doi.org/10.1080/23248378.2023.2228802

[2] Alfredo Peinado Gonzalo, Richard Horridge, Heather Steele, Edward Stewart, and Mani Entezami. Review of data analytics for condition monitoring of railway track geometry. IEEE Transactions on Intelligent Transportation Systems, 23(12):22737-22754, 2022. https://doi.org/10.1109/TITS.2022.3214121

[3] Corentin Lubeigt, Lorenzo Ortega, Jordi Vilà-Valls, Laurent Lestarquit, and Eric Chaumette. Clean-to-composite bound ratio: A multipath criterion for GNSS signal design and analysis. IEEE Transactions on Aerospace and Electronic Systems, 58(6):5412-5424, 2022. https://doi.org/10.1109/TAES.2022.3172023

[4] Shuai Ma, Xb Liu, Bo Zhang, Weile Qiang, and Jianmei Wei. Similarity based position calibration for multisource track inspection data. Proceedings of the Institution of Mechanical Engineers, Part F: Journal of Rail and Rapid Transit, 237(10):1320-1331, 2023. https://doi.org/10.1177/09544097231165087

[5] Xu Sun, Ping Wang, Jingmang Xu, Fei Xu, and Yang Gao. Simulation of the inherent structural

irregularities of high-speed railway turnouts based on a virtual track inspection method. Proceedings of the Institution of Mechanical Engineers, Part F: Journal of Rail and Rapid Transit, 237(1):114-123, 2023. https://doi.org/10.1177/09544097221092616

[6] Long Chen, Peng Xu, and Teng Wang. Metro track geometry car routing problem with periodic demands: a case study in Beijing, China. Engineering Optimization, 56(9):1409-1428, 2024. https://doi.org/10.1080/0305215X.2023.2256228

[7] Tadas Žvirblis, Armantas Pikšrys, Damian Bzinkowski, Mirosław Rucki, Artūras Kilikevičius, and Olga Kurasova. Data augmentation for classification of multi-domain tension signals. Informatica, 35(4):883-908, 2024. https://doi.org/10.15388/24-INFOR578

[8] Yiwei Xu, Kuangang Fan, Qian Hu, and Xuetao Zhang. Positioning of suspended permanent magnet maglev trains using satellite-ground multi-sensor fusion. IEEE Sensors Journal, 24(10):16816-16825, 2024. https://doi.org/10.1109/JSEN.2024.3384699

[9] Felipe Barboza da Silva, Ediz Cetin, and Wallace Alves Martins. Radio frequency interference mitigation via nonnegative matrix factorization for GNSS. IEEE Transactions on Aerospace and Electronic Systems, 59(4):3493-3504, 2022. https://doi.org/10.1109/TAES.2022.3229284

[10] Xiaojun Zou, and Xin Chen. A MEMS-assisted GNSS signal uninterrupted tracking method based on adaptive motion constraints. IEEE Sensors Journal, 24(2):1847-1856, 2023. https://doi.org/10.1109/JSEN.2023.3337174

[11] Kaoru Ichikawa, Jing Qiao Zhu, Joushiro Noda, Ryosuke Sakemi, Kei Yufu, and Kuniaki Matsuura. Ship-borne wave gauge using GNSS interferometric reflectometry. Coastal Engineering Journal, 66(2):395-404, 2024. https://doi.org/10.1080/21664250.2024.2342596

[12] Tarek Hassan, Tamer Fath-Allah, Mohamed Elhabiby, Alaa ElDin Awad, and Mohamed El-Tokhey. Integration of GNSS observations with volunteered geographic information for improved navigation performance. Journal of Applied Geodesy, 16(3):265-277, 2022. https://doi.org/10.1515/jag-2021-0063

[13] Jian Kuang, Dazhou Xia, Tao Liu, Qijin Chen, and Xiaoji Niu. Shin-INS: A shin-mounted IMU-based inertial navigation system for pedestrian. IEEE Sensors Journal, 23(21):25760-25769, 2023. https://doi.org/10.1109/JSEN.2023.3312631

[14] Xiaoli Hao, Jian Yang, Fei Yang, Xianfu Sun, Yali Hou, and Jian Wang. Track geometry estimation from vehicle-body acceleration for high-speed railway using deep learning technique. Vehicle System Dynamics, 61(1):239-259, 2023. https://doi.org/10.1080/00423114.2022.2037669

[15] Tuan Li, Hao Zhang, Bing Han, Ming Xia, and Chuang Shi. Relative accuracy of GNSS/INS integration based on factor graph optimization. IEEE Sensors Journal, 22(15):15334-15344, 2024. https://doi.org/10.1109/JSEN.2024.3451665

[16] Yidi Chen, Wei Jiang, Jian Wang, Baigen Cai, Dan Liu, Xiaohui Ba, and Yang Yang. An LSTM-assisted GNSS/INS integration system using IMU recomputed error information for train localization. IEEE Transactions on Aerospace and Electronic Systems, 60(3):2658-2671, 2023. https://doi.org/10.1109/TAES.2023.3328318

[17] Antoine Baudiquez, and Gianna Panfilo. Automatic detection of anomalies in post-processed data applied to UTC time transfer links. IEEE Transactions on Ultrasonics, Ferroelectrics, and Frequency Control, 71(9):1162-1169, 2024. https://doi.org/10.1109/TUFFC.2024.3434378

[18] Tabish Badar, Simo Särkkä, Zheng Zhao, and Arto Visala. Rao-blackwellized particle filter using noise adaptive kalman filter for fully mixing state-space models. IEEE Transactions on Aerospace and Electronic Systems, 60(5):6972-6982, 2024. https://doi.org/10.1109/TAES.2024.3409644

[19] Chenyan Sun, and Kui Li. A vehicle-carried INS positioning accuracy improvement method by using lateral constraint in GPS-denied environment. IEEE Transactions on Vehicular Technology, 72(1):205-213, 2022. https://doi.org/10.1109/TVT.2022.3205047

[20] Gimin Kim, TaeHyeong Jeon, Jaeyoung Song, Sul-Gee Park, and Sanghyun Park. Architecture design for maritime centimeter-level GNSS augmentation service and initial experimental results on testbed network. Continuity, 11(4):269-277, 2022. https://doi.org/10.11003/JPNT.2022.11.4.269

[21] Jelena Gučević, Siniša Delčev, Miroslav Kuburić, Milan Trifković, and Vukan Ogrizović. Impact of vial bubble on the accuracy of positions in the GNSS-RTK mode. Tehnički Vjesnik, 29(4):1230-1235, 2022. https://doi.org/10.17559/TV-20211214153457

[22] Linxuan Wang, Xiangwei Kong, Hongzhe Xu, and Hong Li. INS-GNSS integrated navigation algorithm based on TransGAN. Intelligent Automation & Soft Computing, 37(1):5654-5663, 2023. https://doi.org/10.32604/iasc.2023.035876

[23] Xinwu Liu, and Wenhui Lian. Restoration of Poissonian images using nonconvex regularizer with overlapping group sparsity. Informatica, 33(3):573-592, 2022. https://doi.org/10.15388/22-INFOR480